Systemic cytokines drive conserved severity-associated myeloid responses across bacterial and viral infections

Check for updates

Kimberly Kajihara[1], Donghong Yan[2], Gretchen L. Seim[1], Hannah Little-Hooy[2], Jing Kang[2], Cynthia Chen[3], Marco De Simone[3], Tim Delemarre[4], Spyros Darmanis[3], Haridha Shivram[5], Rebecca N. Bauer[5], Carrie M. Rosenberger [4], Sharookh B. Kapadia [1], Min Xu [2] & Miguel Reyes [1] ✉

Both bacterial and viral infections can trigger an overwhelming host response, leading to immunopathology and organ dysfunction. Multiple studies have reported dysregulated myeloid cell states in patients with bacterial sepsis or severe SARS-CoV-2 infection. However, their relevance to viral infections other than COVID-19, the factors driving their induction, and their role in tissue injury remain poorly understood. Here, we performed a multi-cohort analysis of single cell and bulk transcriptomic data from 1845 patients across 25 studies. Our meta-analysis revealed a conserved severity-associated gene signature pointing to emergency myelopoiesis (EM) and increased *IL1R2* expression in monocytes and neutrophils from patients with bacterial sepsis, COVID-19, and influenza. Analysis of tocilizumab-treated COVID-19 patients showed that IL-6 signaling blockade partially reduces this signature and results in a compensatory increase in G-CSF. To validate the role of these cytokines in vivo, we used a mouse model of influenza infection that recapitulates severity-associated increases in IL1R2+ monocytes and IL1R2hi neutrophils, and demonstrate that combined IL-6 and G-CSF blockade inhibits their production. Our study demonstrates the cooperative role of G-CSF and IL-6 in driving the production of severity-associated IL1R2+ myeloid cells and highlights the link between myeloid dysregulation and tissue injury during severe infection.

Sepsis accounts for one in five deaths globally and is characterized by a dysregulated host response to infection leading to multi-organ dysfunction[1]. The recent SARS-CoV-2 pandemic and prior influenza outbreaks also highlight the potential for viruses to cause severe disease leading to hospitalization or mortality. Despite the lung being the primary infection site of SARS-CoV-2, severe cases of COVID-19 may involve extra-pulmonary organ dysfunction, mirroring key manifestations of sepsis[2]. In both sepsis and COVID-19 patients, biomarkers of tissue injury, such as cfDNA, are associated with disease severity and are prognostic for intensive care need and mortality[3–5]. To prepare for future infectious disease outbreaks[6], there is a need to develop therapeutics that limit tissue injury resulting from severe infection by various pathogens.

Traditionally, pathogen-directed therapies are the first-line strategy against infectious diseases. However, the effectiveness of antibiotics is increasingly compromised by the rise of antimicrobial resistance[7], while existing antivirals have a narrow spectrum of activity and are often ineffective in patients with severe disease[8–11]. In contrast, host-directed therapies (HDTs) can offer a pathogen-agnostic approach, eliminating the need for pathogen identification and providing a significant advantage for pandemic preparedness[12]. Therapies targeting the host inflammatory response have shown benefit in reducing mortality and hospitalization in patients with severe COVID-19. Understanding the commonalities between the host response to viral and bacterial sepsis, and its role in the development of tissue injury, will be essential for the development of HDTs that can be applied across a range of infectious diseases[13,14].

Several studies have reported profound transcriptional and immunophenotypic alterations, particularly in myeloid cells, in patients with bacterial sepsis and severe viral disease[15–21]. These studies highlight the

[1]Department of Infectious Diseases, Genentech, South San Francisco, CA, USA. [2]Department of Translational Immunology, Genentech, South San Francisco, CA, USA. [3]Department of Microchemistry, Proteomics, Lipidomics and Next-Generation Sequencing, Genentech, South San Francisco, CA, USA. [4]Department of Immunology and Regenerative Medicine, Genentech, South San Francisco, CA, USA. [5]Department of Translational Medicine, Genentech, South San Francisco, CA, USA. ✉e-mail: reyes.miguel@gene.com

expansion of immature monocytes, neutrophils, and myeloid progenitors in circulation, commonly referred to as emergency myelopoiesis (EM)[22]. We previously described the expansion of MS1 monocytes (IL1R2 + HLA-DR[low]) in both bacterial sepsis and severe COVID-19[21,23,24]. These cells can be induced in vitro by treatment of human hematopoietic stem and progenitor cells (HSPCs) with plasma from patients with sepsis or severe COVID-19[23], indicating a role for EM in its induction. Recently, EM has also been proposed as a driver of severity-associated immature neutrophils in sepsis and COVID-19[25–27]. The relevance of these cell states to non-COVID-19 viral infection and the factors driving their induction remain unclear. Importantly, their role in tissue injury and organ dysfunction has not been established. In this study, we show that transcriptional signatures of EM are associated with disease severity across bacterial sepsis, severe COVID-19, influenza, and RSV. We identified cytokines that drive these signatures in humans and characterized the role of severity-associated monocytes and neutrophils in tissue injury in vivo.

Results

Large-scale meta-analysis identifies shared monocyte and neutrophil gene programs in sepsis and severe COVID-19

We previously performed a meta-analysis of blood monocytes from 5 scRNA-seq datasets to demonstrate the expansion of MS1 monocytes in both sepsis and severe COVID-19[23]. To validate these findings and identify shared transcriptional programs across myeloid cells, we expanded this analysis to 19 datasets[16,17,21,23,25–38], including 6 studies with transcriptional data from blood neutrophils (Fig. 1a, *Methods*, Supplementary Table 1). Our expanded meta-analysis of monocytes identified gene programs shared across datasets, including the MS1 and MHC-II gene programs (Supplementary Fig. 1). Consistent with our previous findings, we found that, across all datasets, usage of the MS1 and MHC-II gene programs are increased and decreased, respectively, in sepsis patients compared to healthy controls, and in severe compared to mild COVID-19 (Fig. 1b, c, Supplementary Figs. 1, 2, Supplementary Table 2, Supplementary Data 1). Of note, MS1, but not MHC-II, gene program
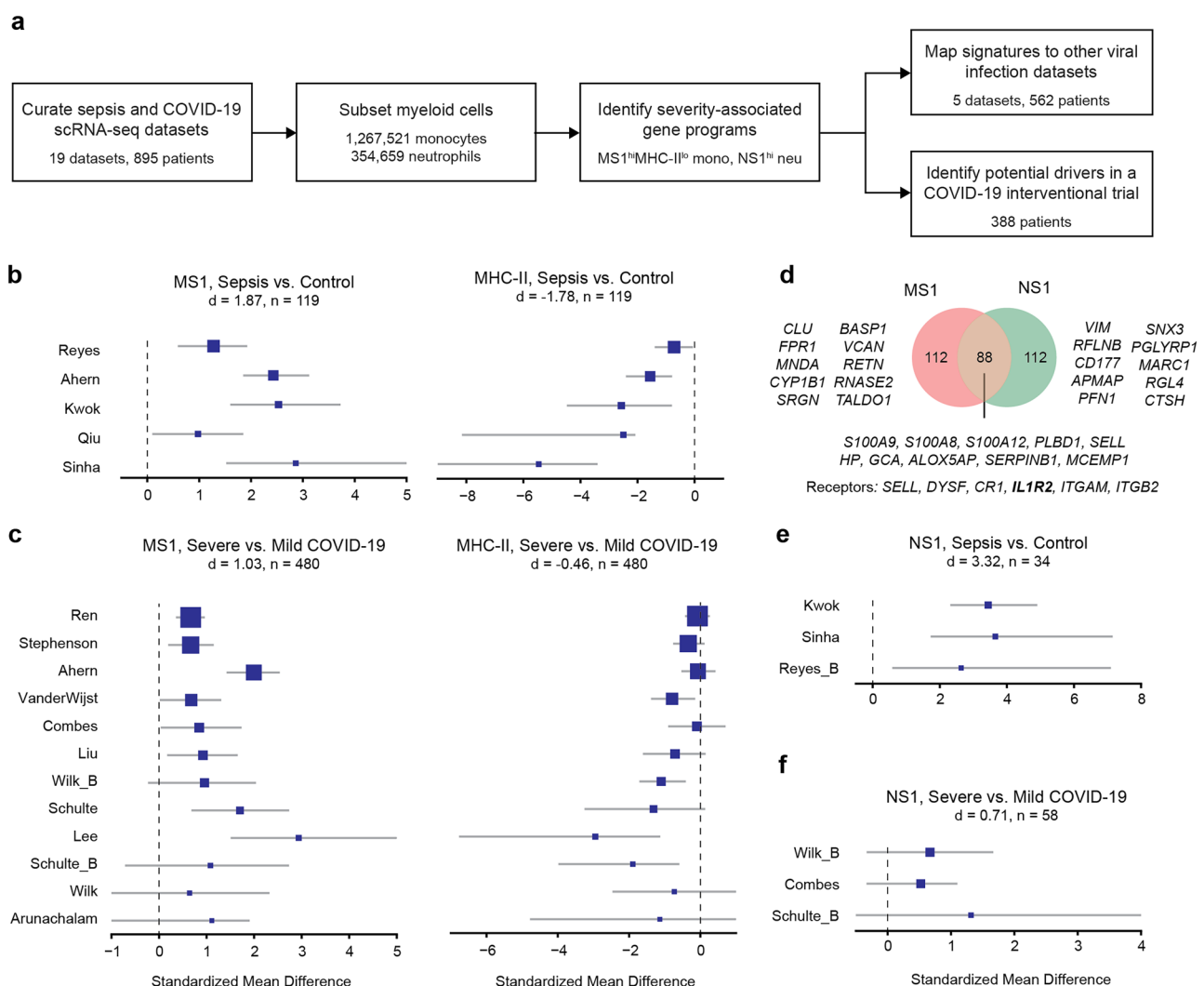
Fig. 1 | Emergency myelopoiesis gene programs are associated with sepsis and COVID-19 severity. a Analysis scheme for 18 scRNA-seq datasets and 6 bulk transcriptomics datasets from cohorts of patients with bacterial sepsis, COVID-19, or non-COVID-19 viral infection. **b, c, e, f** Forest plots indicate the effect sizes (log2 standardized mean difference) across datasets for each indicated gene program. Blue boxes indicate the effect size in an individual study, with whiskers extending to the 95% confidence interval. Size of each box is proportional to the relative sample size of the study. Detailed descriptions of the patient cohorts, numbers of cells and patients for each dataset, and sampling methods are described in the corresponding publications[16,17,21,23,25–38] and summarized in Supplementary Table 1. **d** Venn diagram showing the overlap between the top 200 genes in the MS1 and NS1 programs. The top ten genes with highest loadings in each region are indicated. Genes in both programs that encode cell surface receptors are also indicated.

usage in monocytes was associated with mortality among patients with sepsis or severe COVID-19 (Supplementary Fig. 2c).

We performed a meta-analysis of blood neutrophils (Supplementary Fig. 3a, d), and identified a neutrophil program, which we named NS1, that shares several genes with the MS1 monocyte program, including the gene encoding the receptor *IL1R2* (Fig. 1d, Supplementary Data 2). NS1 is similarly upregulated in sepsis and severe COVID-19, though with a smaller effect size when comparing mild vs. severe COVID-19 (Fig. 1e, f, Supplementary Fig. 3c, d, Supplementary Table 2). Usage of the MS1 and NS1 gene programs across patients correlated significantly in 3 out of 5 datasets with both cell types, suggesting that these gene programs may be driven by similar pathways (Supplementary Fig. 3e). Of note, the top genes of the NS1 program also point to EM, as the expression of granule genes in blood neutrophils are indicative of premature release of developing neutrophils[39]. In addition, we found significantly increased *IL1R2* expression in sepsis and severe COVID-19 patients in the majority of datasets analyzed (monocytes: 11 of 18, neutrophils: 4 of 6 datasets; Supplementary Fig. 4). Our meta-analysis shows that EM-associated gene programs and *IL1R2* can be detected in both monocytes and neutrophils, and their increased expression in both cell types is associated with sepsis and COVID-19 severity.

### EM gene programs and IL1R2 increase with severity in non-COVID-19 viral infection

Given the increased expression of EM-associated gene programs in both sepsis and severe COVID-19, we hypothesized that similar patterns will be observed in non-COVID-19 respiratory infections, including influenza and RSV. We used the top genes associated with each consensus gene program from our meta-analysis (MS1, MHC-II, and NS1) to estimate the expansion of EM-associated cell states in bulk whole blood transcriptomic datasets (*Methods*, Supplementary Table 3). Interestingly, we found that EM scores significantly increase with disease severity in 3 out of 4 influenza datasets

and in RSV (Fig. 2a, b), with a summary effect size of 1.58 across all datasets (Fig. 2c, Supplementary Table 4). Consistent with this result, usage of MS1 and MHC-II are increased and decreased, respectively, in two scRNA-seq datasets that included cohorts of patients with severe influenza (Supplementary Fig. 1c, d, 2a, b). In addition, we found that expression of *IL1R2* is significantly increased in 3 out of 4 influenza datasets, but not in RSV, with a summary effect size of 0.93 across all datasets. These results suggest that the EM signatures and *IL1R2* expression also increase in severe influenza and, to a lesser extent, RSV.

EM signatures are partially reduced by IL6 signaling blockade

We previously demonstrated that the induction of MS1 monocytes in HSPCs by sepsis plasma is partially mediated by IL-6[23]. To confirm the role of IL-6 in MS1 induction in COVID-19 patients, we analyzed published bulk transcriptional data from COVACTA: a phase 3 randomized placebo-controlled study of tocilizumab, an anti-IL-6R antibody, in hospitalized COVID-19 patients[15,40]. Consistent with our findings from the meta-analysis, we found that both EM scores and *IL1R2* expression increase with baseline ordinal severity (Supplementary Fig. 5a, b). In addition, higher EM scores and *IL1R2* expression at baseline were significantly associated with mortality and mechanical ventilation on day 28 in placebo-treated patients (PBO; Fig. 3a). Importantly, we found that tocilizumab-treated patients (TCZ) have a greater reduction in EM scores compared with the PBO group on days 3 and 7 after treatment (Fig. 3b), confirming the role of IL-6 signaling in inducing EM in COVID-19 patients. Of note, patients who are still mechanically ventilated (MV) at day 28 had significantly higher EM scores, independent of treatment, indicating that IL-6 signaling blockade is not sufficient to completely inhibit EM in patients with critical COVID-19.

To identify other potential EM drivers besides IL-6, we analyzed correlations between blood protein levels and leukocyte gene expression in TCZ-treated patients. We identified several proteins whose increase in
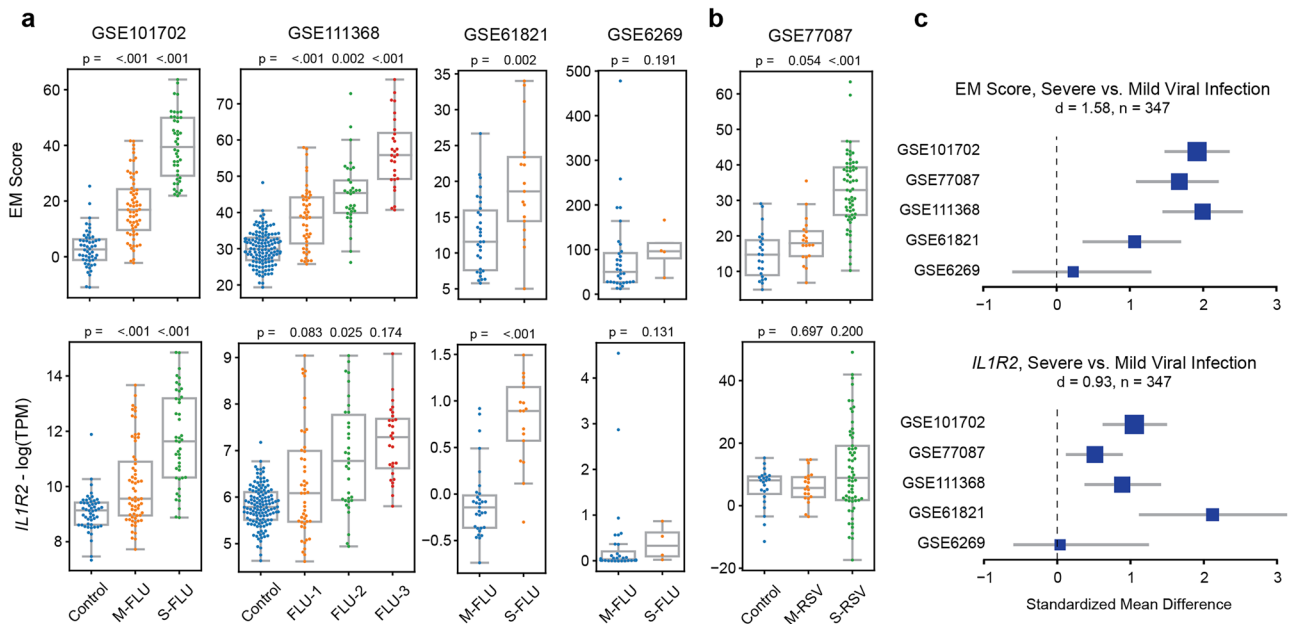
Fig. 2 | Emergency myelopoiesis signatures and *IL1R2* expression increase with severity in non-COVID-19 viral infection. EM scores (top) and *IL1R2* expression (bottom) in blood transcriptional datasets of influenza (a) and RSV (b) patients. Boxes show the median and interquartile range (IQR) for each patient cohort, with whiskers extending to 1.5 IQR in either direction from the top or bottom quartile. Accession numbers for each dataset are indicated above. *p* values shown are calculated by comparing each disease state with Control (GSE101702 and GSE111368) or M-FLU group (GSE61821 and GSE6269) using a two-tailed Wilcoxon rank-sum test. Detailed descriptions of the patient cohorts and numbers of patients for each dataset are described in the corresponding publications[18,19,55–57] and listed in

Supplementary Table 2. **c** Forest plots indicate the effect sizes (log2 standardized mean difference) of the EM score (top) and *IL1R2* expression (bottom) between mild vs. severe patients across datasets. Accession numbers for each dataset are indicated on the left. Blue boxes indicate the effect size in an individual study, with whiskers extending to the 95% confidence interval. Size of each box is proportional to the relative sample size of the study. M-FLU mild influenza, S-FLU severe influenza, FLU-1 influenza with no supplemental oxygen required, FLU-2 influenza with oxygen by mask required, FLU-3 influenza with mechanical ventilation. M-RSV mild respiratory syncytial virus infection, S-FLU severe respiratory syncytial virus infection.
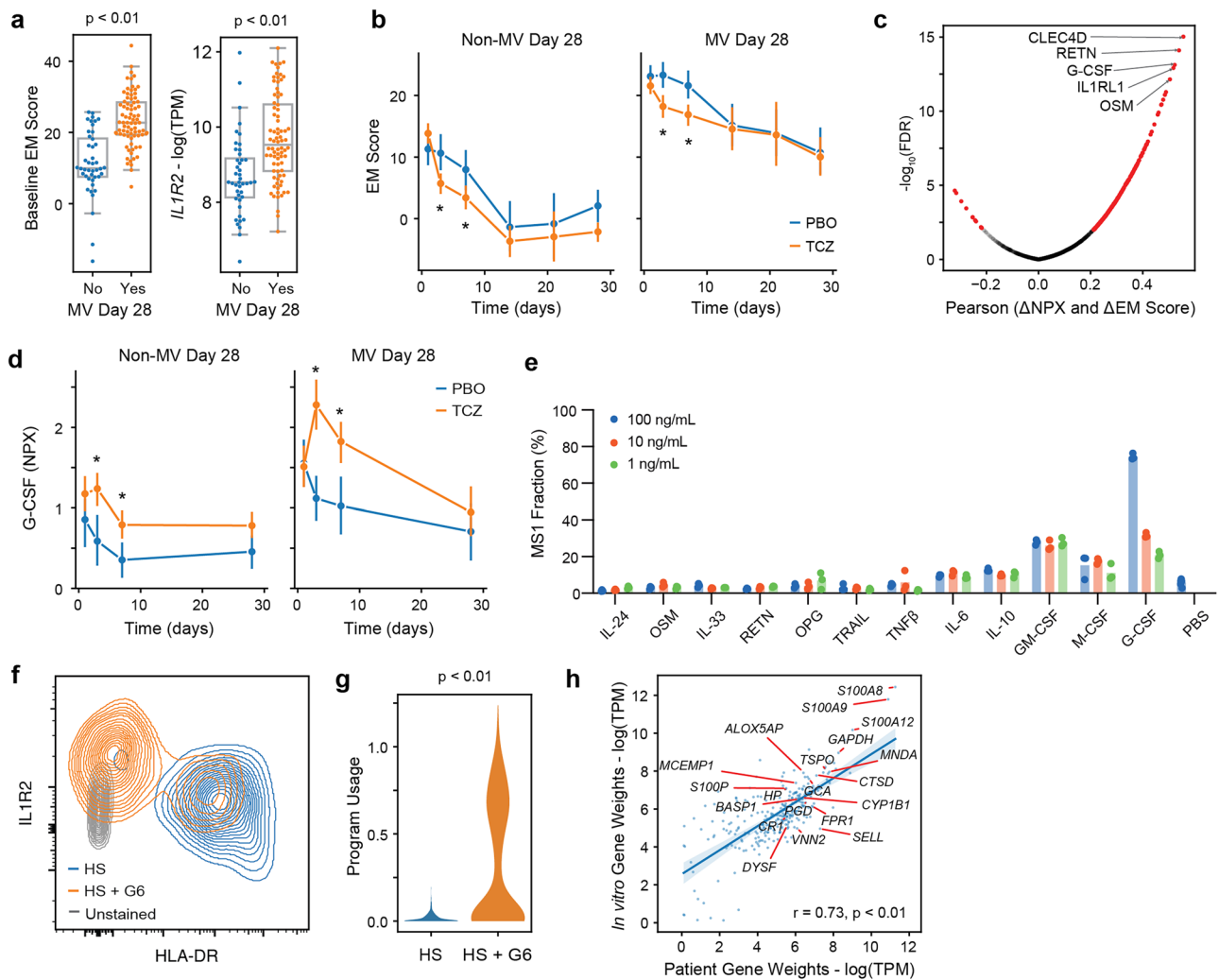
Fig. 3 | IL-6 and G-CSF drive emergency myelopoiesis and production of MS1 monocytes. a EM scores (left) and *IL1R2* expression (right) in patients from the PBO arm of COVACTA grouped by mechanical ventilation status on day 28. Boxes show the median and interquartile range (IQR) for each patient cohort, with whiskers extending to 1.5 IQR in either direction from the top or bottom quartile. *p* values shown are calculated for each comparison using a two-tailed Wilcoxon rank-sum test. **b** EM scores over time in patients from the PBO or TCZ arm of COVACTA, grouped by mechanical ventilation status. EM scores are averaged across all patients for each group and timepoint. Error bars indicate the 95% confidence interval of the mean. Asterisks indicate a false discovery rate (FDR) < 0.05, computed by comparing the PBO and TCZ group at each timepoint (two-tailed Wilcoxon rank sum test, corrected for multiple testing). **c** Volcano plot showing the Pearson correlation between changes in protein levels and changes in EM score from baseline to day 3 in the TCZ group. Significance of each correlation was calculated with a two-sided permutation test. Proteins with FDR of <0.01 are highlighted in red. **d** G-CSF levels over time in patients from the PBO or TCZ arm of COVACTA, grouped by

mechanical ventilation status. G-CSF levels are averaged across all patients for each group and time point. Error bars indicate the 95% confidence interval of the mean. Asterisks indicate a false discovery rate (FDR) < 0.05, computed by comparing the PBO and TCZ group at each timepoint (two-tailed Wilcoxon rank sum test, corrected for multiple testing). **e** Fraction of MS1 (IL1R2 + HLA-DR^{low}) among monocytes in HSPCs incubated with each cytokine at the indicated concentration (*n* = 3 replicates for each cytokine and concentration). **f** Flow cytometry density plot of CD14+ monocytes from HSPCs treated with healthy serum (HS) or healthy serum with 10 ng/mL IL-6 and G-CSF (HS + G6) (representative across 3 experiments). **g** Violin plot of MS1 gene program usage in monocytes differentiated from HSPCs treated with HS or HS + G6. **h** Gene weight correlation between the MS1 program detected in patients (x-axis) and the MS1 program detected in differentiated HSPCs (y-axis). Significance of the Pearson correlations (r) was calculated with a permutation test. The top 20 genes with the highest z-score loadings in the patient MS1 program are labeled. NPX normalized protein expression.

expression from baseline to day 3 are significantly correlated with increases in EM scores (Fig. 3c, Supplementary Data 3). Among the top proteins was G-CSF, a cytokine that plays a key role in granulocyte production[41,42]. Of note, G-CSF levels significantly increase with TCZ treatment in COVACTA as we reported previously[40], and changes in both G-CSF and EM scores are higher in patients who are MV at day 28 (Fig. 3d, Supplementary Fig. 5c). While both changes in IL-6 and G-CSF correlate with EM in the PBO group, G-CSF has a stronger correlation with EM in the TCZ group (Supplementary Fig. 5d). In addition, both G-CSF and IL-6 levels are correlated with sRAGE, a marker of lung epithelial tissue injury that is associated with severity and poor outcomes in COVID-19 (Supplementary Fig. 5f, g). These

data suggest that G-CSF is another driver of myeloid inflammation and tissue injury in COVID-19 patients, and that IL-6 signaling blockade may result in a compensatory increase in G-CSF that maintains elevated EM signatures, particularly in critical COVID-19 patients.

G-CSF and IL-6 induce neutrophil and MS1 monocyte production
To test candidate EM drivers, we incubated human HSPCs with cytokines that correlated with EM in our analysis of COVACTA, and measured their effect on total monocyte, MS1, and neutrophil production using flow cytometry (*Methods*). We tested these proteins along with IL-6, IL-10, GM-CSF, and M-CSF, which we previously showed induces MS1 production in

combination[23]. Among the cytokines we tested, G-CSF produced the highest number of neutrophils and monocytes, and specifically induced monocytes with the MS1 immunophenotype (IL1R2 + HLA-DR^low; Fig. 3e, Supplementary Fig. 6a). Interestingly, while higher concentrations of G-CSF and IL-6 induced greater MS1 production in combination, IL-6 slightly reduced neutrophil production in the presence of G-CSF (Fig. 3f, Supplementary Fig. 6b, c).

We performed scRNA-seq on HSPCs differentiated with IL-6 and G-CSF to confirm the induction of MS1 monocytes by gene expression (Supplementary Fig. 7a). We found increased and decreased expression of MS1 and MHC-II genes, respectively, in CD14+ cells generated from HSPCs with IL-6 and G-CSF compared with healthy serum alone (Supplementary Fig. 7b, c). Unbiased analysis of the in vitro scRNA-seq data also detected gene programs similar to MS1 and MHC-II in patients, and their usage patterns are consistent with those observed in sepsis and COVID-19 (Fig. 3g, h, Supplementary Fig. 7d–f). Altogether, these data suggest that both G-CSF and IL-6 could induce EM signatures observed in patients, and that their combination is sufficient to produce MS1 monocytes in vitro.

EM signatures are recapitulated by influenza infection in mice

To confirm the role of these cytokines and understand the roles EM-associated cell states in vivo, we utilized a mouse model of influenza A/PuertoRico/8/34 H1N1 (PR8) infection. Given the association of EM signatures with influenza severity in humans (Fig. 2a), we first evaluated the relationship between EM signatures and infection dose (Fig. 4a). While we did not find dose-dependent differences in the absolute number of monocytes in the blood and BALF, we found a specific increase in IL1R2+ monocytes (Fig. 4b–d, Supplementary Fig. 8a). In addition, we found a significant increase in IL1R2 expression among neutrophils with higher infection dose (Fig. 4e, f, Supplementary Fig. 8b). Similar to patients with severe COVID-19, levels of G-CSF and IL-6 in the blood are elevated with PR8 infection, and their levels significantly correlate across individual mice (Supplementary Fig. 8c, d). We also found significant increases in G-CSF and IL-6 in the BALF, but their levels are not correlated (Supplementary Fig. 8e, f). These data suggest that monocyte and neutrophil states at higher infection doses are similar to those found in patients with severe infection.

To confirm the presence of EM signatures in vivo by gene expression, we performed scRNA-seq on blood and BALF immune cells from PR8-infected mice (Supplementary Fig. 9a, b). Prior to analysis, we converted mouse to human genes in the scRNA-seq data to enable the quantification of our human signatures in vivo (*Methods*). Similar to the patterns observed in humans, we found increasing expression of the MS1 and NS1 genes in mouse monocytes and neutrophils, respectively, with higher infection dose (Supplementary Fig. 8c). In addition, unbiased cNMF analysis revealed gene programs similar to MS1 and NS1, and their usages increased with higher infection dose (Supplementary Fig. 9d–g). Altogether, these data suggest that EM signatures and their severity-associated increases in humans can be modeled by high-dose PR8 infection in mice.

Combined IL-6 and G-CSF signaling blockade inhibits EM in vivo

Given the associations of IL-6 and G-CSF with EM signatures in patients and their effect in inducing EM in vitro, we tested the effects of blocking these cytokines or their receptors during high-dose PR8 infection in vivo (Fig. 4g–m, Supplementary Fig. 10a–f). As expected, treatment with α-G-CSF or α-IL-6R resulted in a decrease in G-CSF and increase in IL-6 levels, respectively (Supplementary Fig. 10b). While a combination of α-G-CSF and α-IL-6R was necessary to observe a significant decrease in BALF monocytes (Fig. 4h), α-G-CSF or α-IL-6R alone significantly reduced the number of IL1R2+ monocytes, and their combination resulted in an even greater numerical decrease in the BALF (Fig. 4i). Similarly, α-G-CSF, α-IL-6R, and their combination significantly reduced the number of IL1R2+ monocytes in the blood (Supplementary Fig. 10d). α-G-CSF alone and its combination with α-IL-6R also reduced neutrophil numbers in both BALF and blood (Fig. 4j, Supplementary Fig. 10e). However, their effects on

reducing neutrophil IL1R2 expression were only observed in the BALF, suggesting that other factors beyond G-CSF and IL-6 may control neutrophil IL1R2 expression in the blood (Fig. 4k, Supplementary Fig. 10f). Altogether, these findings confirm the role of IL-6 and G-CSF signaling in inducing both EM-associated monocytes and neutrophils, particularly in the lung, during severe influenza infection in vivo.

To assess the consequence of targeting EM on tissue injury in vivo, we measured biomarkers of broad tissue injury (cell-free DNA)[3,4] and epithelial injury (sRAGE)[43,44] in the BALF. Individual treatment with α-G-CSF or α-IL-6R resulted in nominal reduction of cfDNA levels, while their combination resulted in a significant decrease (Fig. 4l). Interestingly, despite the correlation of G-CSF and IL-6 with sRAGE in patients, we did not observe a significant reduction in sRAGE with α-G-CSF, α-IL6-R, or their combination (Fig. 4m). No significant changes in body weight loss were also observed across the treatment groups (Supplementary Fig. 10a). These results suggest that inhibiting EM can broadly reduce tissue injury, but may have a limited effect in preventing epithelial injury in the lung.

Cell type-specific effects of EM on tissue injury in vivo

Given the presence of EM signatures in both monocytes and neutrophils, we sought to understand the role of each myeloid cell type on tissue injury. To test the role of EM-induced monocytes in vivo, we performed high-dose PR8 infection in Ccr2-/- mice (Fig. 5a). Ccr2 deletion resulted in significant decreases in numbers of both total monocytes and IL1R2+ monocytes, but not neutrophils (Fig. 5b–d). Strikingly, we found that PR8 infection in Ccr2-/- mice resulted in increased levels of both tissue injury markers, cfDNA and sRAGE (Fig. 5e, f). These increases are not associated with changes in body weight nor defects in pathogen control, as viral titers are similar between WT and Ccr2-/- mice (Fig. 5g, Supplementary Fig. 10g). Conversely, we used antibody-mediated depletion to understand the role of neutrophils during EM (Fig. 5h). α-Gr1 treatment initiated on days 1 or 3 post-infection resulted in near-complete elimination of neutrophils on day 7 (Fig. 5k). anti-Gr1 also resulted in partial reduction of monocyte numbers; however, the number of IL1R2+ monocytes were unaffected (Fig. 5i, j). Consistent with the known tissue-damaging effects of neutrophils, we found significant reductions in both cfDNA and sRAGE levels in anti-Gr1 treated mice (Fig. 5l, m), however, we did not observe changes in body weight nor viral titer (Fig. 5n, Supplementary Fig. 10i). Interestingly, we found significant increases in G-CSF and IL-6 in both Ccr2-/- mice and α-Gr1 treated mice (Supplementary Fig. 10h, j), suggesting a potential compensatory myelopoietic response in response to depletion of either cell type.

Altogether, these results show that neutrophils are the primary mediators of tissue damage while monocytes may play a beneficial role during EM. Importantly, these findings suggest that completely inhibiting EM may not be efficacious in influenza, as it may limit not only tissue injury caused by neutrophils, but also the beneficial effect of IL1R2+ monocytes.

Discussion

Our study demonstrates that EM-associated cell states are expanded across severe bacterial and viral infections in humans. By performing a meta-analysis of published single cell and bulk transcriptional datasets, we show that gene programs associated with EM are upregulated in sepsis patients and correlated with severity in patients with SARS-CoV-2, RSV, or influenza infection. These findings are consistent with a recent report identifying conserved severity-associated gene modules, including myelopoiesis, across multiple viruses[45]. Our analysis has a number of limitations. Only one RSV dataset was included in our meta-analysis, so limited conclusions can be drawn on the relevance of EM to RSV. In addition, quantification of EM gene programs in patients with non-COVID-19 viral infection was limited to bulk transcriptional datasets in our study, and additional scRNA-seq data are needed to specifically confirm the up-regulation of EM gene programs in blood neutrophils and monocytes from influenza and RSV-infected patients. Our meta-analysis was also limited to blood samples. While previous reports have also noted the presence of MS1 monocytes and IL1R2+ neutrophils in the airways of COVID-19 patients[23,46], additional
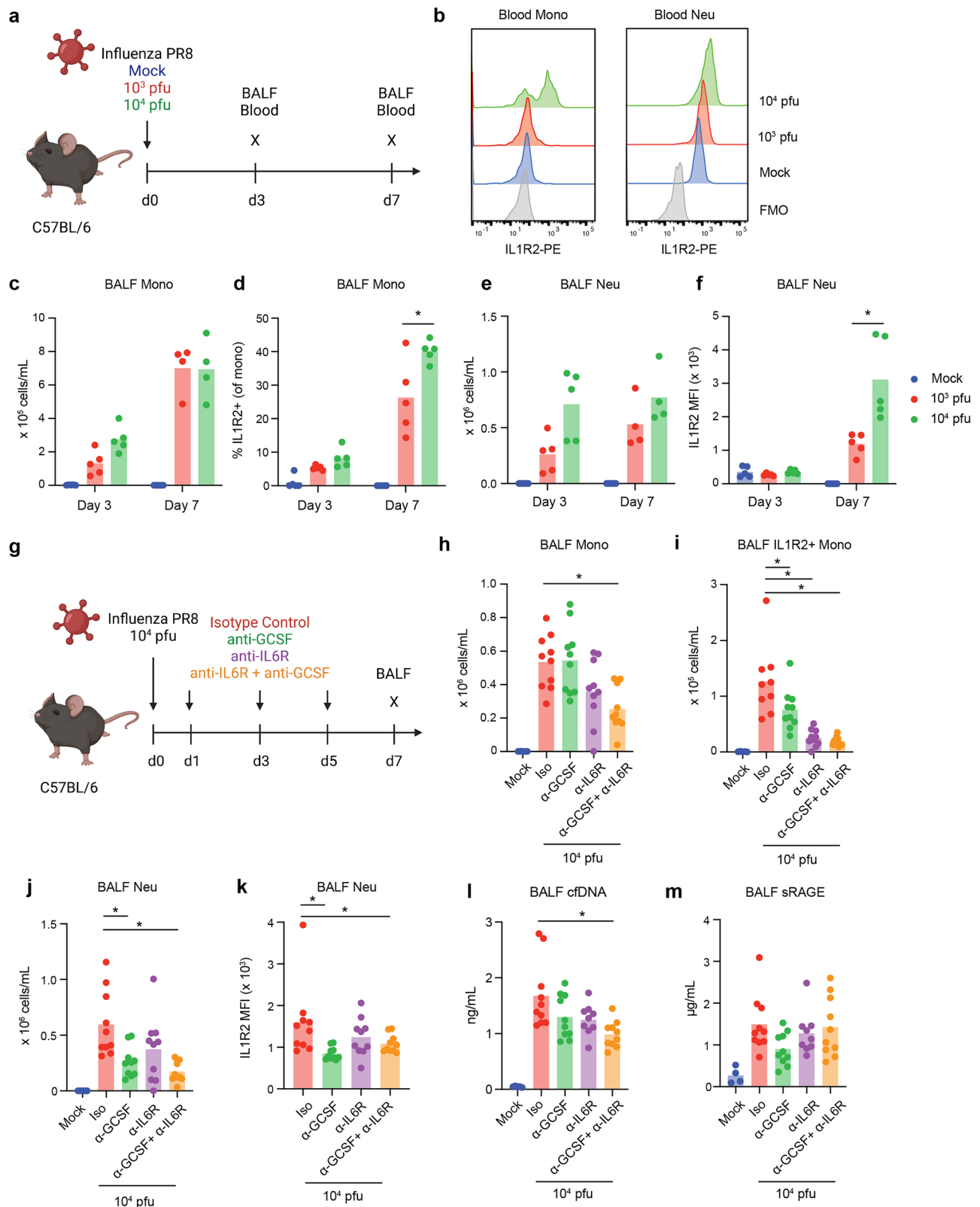
Fig. 4 | IL-6 and G-CSF drive emergency myelopoiesis during severe influenza infection in vivo. a Schematic of the influenza dose titration experiment ($n = 5$ mice for each dose and timepoint). Figure created with Biorender.com (**b**) IL1R2 surface expression at day 7 post-infection in monocytes (left) and neutrophils (right) in the blood of mice infected with the indicated PR8 titer. **c** Number and **d** fraction of IL1R2+ blood monocytes in mice infected with PR8 at the indicated time point. **e** Number and **f** IL1R2 mean fluorescence intensity (MFI) of blood neutrophils in mice infected with PR8 at the indicated time point. **g** Schematic of the IL6 and G-CSF blockade experiment ($n = 5$ for mock infection, $n = 10$ mice for infected and antibody-treated groups). **h** Number of total monocytes, **i** IL1R2+ monocytes, **j** neutrophils, and **k** neutrophil IL1R2 mean fluorescence intensity (MFI) at day 7 post-infection in the BALF of mice infected with 10^4 pfu PR8 and treated with the indicated antibodies. **l** cfDNA and **m** sRAGE levels at day 7 post-infection in the BALF of mice infected with 10^4 PR8 and treated with the indicated antibodies. Asterisks indicate a significant difference (FDR < 0.05, Mann-Whitney test with Benjamini-Hochberg correction for multiple comparisons). BALF bronchoalveolar lavage fluid, Iso isotype control.
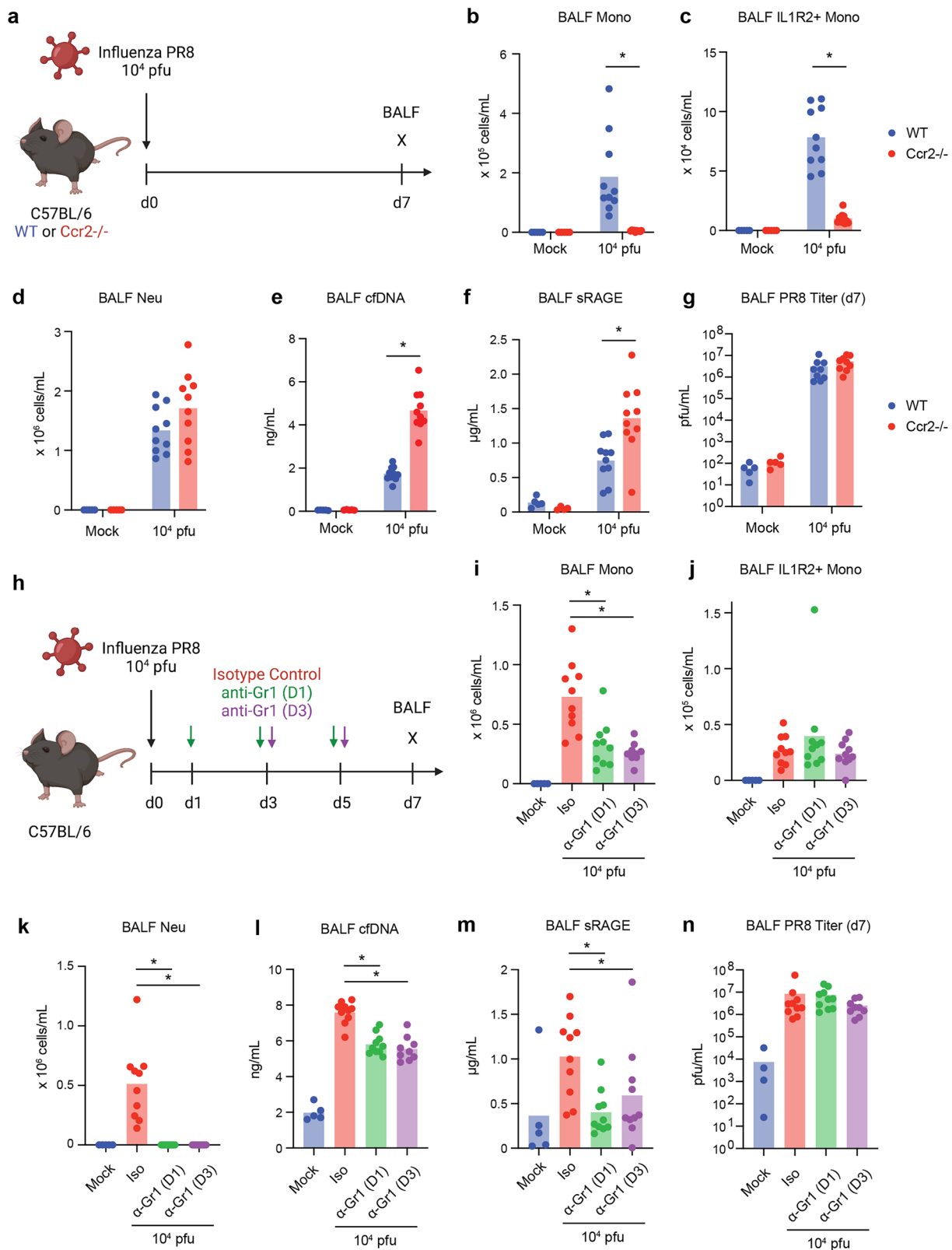
Fig. 5 | Opposing effects of monocytes and neutrophils on tissue injury during severe influenza infection in vivo. a Schematic of the Ccr2-/- influenza experiment (*n* = 5 for mock infection, *n* = 10 mice for infected groups). Figure created with Biorender.com **b** Number of total monocytes, **c** IL1R2+ monocytes and **d** neutrophils at day 7 post-infection in the BALF of wild type (blue) or Ccr2-/- (red) mice infected with 10^4 pfu PR8. **e** cfDNA, **f** sRAGE, and **g** PR8 levels at day 7 post-infection in the BALF of wild type (blue) or Ccr2-/- (red) mice infected with 10^4 pfu PR8. **h** Schematic of the neutrophil depletion experiment (*n* = 5 for mock infection,

n = 10 mice for infected and antibody-treated groups). **i** Number of total monocytes, **j** IL1R2+ monocytes and **k** neutrophils at day 7 post-infection in the BALF of mice infected with 10^4 pfu and treated with α-Gr1. **l** cfDNA, **m** sRAGE, and **n** PR8 levels at day 7 post-infection in the BALF of mice infected with 10^4 pfu and treated with α-Gr1. Asterisks indicate a significant difference (FDR < 0.05, Mann-Whitney test with Benjamini-Hochberg correction for multiple comparisons). BALF bronchoalveolar lavage fluid, Iso isotype control.

confirmatory studies are needed to confirm the presence of these cells in lungs of patients with severe influenza.

Using data from a previous clinical trial and in vitro experiments, we show that EM-associated cell states can be induced by G-CSF and IL-6. In addition, we show that combined targeting of G-CSF and IL-6 reduces EM-associated IL1R2+ monocytes and IL1R2^{hi} neutrophils in a mouse model of severe influenza infection. Interestingly, both cytokines have been proposed as prognostic biomarkers for influenza-associated pneumonia in humans[47]. While G-CSF levels did not correlate with baseline severity or mortality in COVACTA, G-CSF levels at baseline were significantly associated with mechanical ventilation at day 28 (Supplementary Fig. 5e). Our analysis also highlights the compensatory increase in G-CSF in patients treated with TCZ and its correlation with EM scores. The mechanism driving this response in humans, including the cell types that respond to IL-6R blockade and lead to increased G-CSF secretion, remains unknown. In addition, the specific bone marrow precursors that are mobilized by G-CSF and IL-6 to produce IL1R2+ monocytes and IL1R2^{hi} neutrophils remain to be identified. Finally, we show that combined blockade of IL-6 and G-CSF significantly reduces broad tissue injury, as measured by cfDNA, but not epithelial injury, as measured by sRAGE. This suggests that the effects of EM-associated myeloid cells on tissue injury may be cell type-specific, warranting further studies of the interaction of IL1R2+ myeloid cells with various cell types in the lung and other tissues.

Using Ccr2-deficient mice and antibody-mediated neutrophil depletion, we show the opposing effects of monocytes and neutrophils on severe infection-induced tissue injury, independent of their role in pathogen control. Greater neutrophil infiltration and activation in the airways are associated with disease severity in COVID-19[46,48], and pre-clinical studies have demonstrated the role of neutrophil extracellular traps in driving tissue injury[49,50]. Given the tissue-damaging effects of neutrophils, the production of immunosuppressive IL1R2+ monocytes perhaps acts as a negative feedback mechanism to limit neutrophil-mediated tissue injury. Consistent with this hypothesis, it has been reported that G-CSF and IL-6 also induce monocytic myeloid-derived suppressor cells in the context of cancer and allotransplantation[51,52]. While our results demonstrate the opposing roles of total monocytes and neutrophils during severe infection in vivo, the effect of specifically depleting IL1R2+ monocytes or IL1R2^{hi} neutrophils needs to be determined. Nevertheless, our findings highlight the importance of cell-specific targeting to modulate the host response during infection, as myeloid cells may play both detrimental and protective roles.

Overall, our study reveals the drivers of dysregulated myeloid cells during severe infection and their contribution to tissue injury. Our meta-analysis across various infectious diseases suggests that these responses are conserved across multiple pathogens, and that findings from our study may be leveraged to guide the development of diagnostics and therapeutics for future outbreaks.

Methods
Meta-analysis of published scRNA-seq and bulk transcriptional datasets
We searched gene expression databases (GEO, EGA, Single Cell Portal, and Array Express) for publicly available datasets with whole blood or PBMC scRNA-seq data from sepsis and COVID-19 patients. To enable comparisons across disease severity, only datasets with appropriate controls or multiple severity groups (as defined by WHO, NIH, or Berlin ARDS criteria for COVID-19) were included in the analysis (Supplementary Table 1). Filtered gene expression matrices, including their patient and cohort annotations, were obtained from each publication and analyzed using scanpy v1.9.1 and cNMF v1.4.1. We first subsetted monocytes and/or neutrophils from each dataset by using annotations provided by each study. If annotations were unavailable, we performed Leiden clustering and identified monocyte and neutrophil clusters by expression of *LYZ, CD14, CSF3R,* and *S100A8.* After subsetting, we performed cNMF on each individual gene expression matrix with the following parameters: $k = 15$, n-iter = 10, numgenes = 5000 and local-density-threshold = 0.2. To exclude

gene programs from contaminating cell types or those which are lowly expressed, we employed an additional filter and removed programs whose mean usage across all cells is <0.01.

Once cNMF results were obtained from each individual dataset, we identified common gene programs by concatenating and clustering the gene spectra matrices from all datasets. We used hierarchical clustering (scipy v1.10.0) on the concatenated gene spectra matrix with the following parameters: method = "average", metric = "correlation". To identify the top genes in each program cluster, we averaged the gene spectra scores across the programs and ranked the genes by these values. We identified the MS1 and NS1 gene programs by the presence of the genes *S100A8, S100A9, S100A12,* and *ALOX5AP* among the top 10. Similarly, we identified the MHC-II programs by the presence of *HLA-DRA* and *CD74.* We then calculated the mean usage of each gene program for each patient and compared these usage values across patient groups.

Whole blood bulk transcriptomic data from influenza and RSV patients were obtained from a prior meta-analysis[45]. To quantify the EM score in bulk transcriptional datasets, we obtained gene expression matrices from each individual study (Supplementary Table 3). EM scores were calculated as the sum of the top 10 shared MS1 and NS1 genes (*S100A8, S100A9, S100A12, PLBD1, SELL, HP, GCA, ALOX5AP, MCEMP1,* and *TSPO*) subtracted by the sum of the top 10 MHC-II genes (*HLA-DRA, CD74, HLA-DPB1, HLA-DQA1, HLA-DRB1, HLA-DPA1, HLA-DQB1, EEF1A1, HLA-DRB5,* and *HLA-DMA*). Serum protein abundance measurements (Olink Proteomics) and patient level clinical data from the COVACTA clinical trial were also obtained from a prior publication[40].

Meta-analysis across datasets were performed as follows: for each contrast, we first computed the standardized median difference (difference in means normalized by pooled standard deviation) for each dataset, and calculated 95% confidence intervals by bootstrapping the data. Summary effect sizes were then calculated by calculating a weighted average (based on the number of patients for each study) of each effect size.

HSPC differentiation, culture, and flow cytometry
Frozen adult CD34+ bone marrow progenitor cells (0.5 or 1 M aliquots) were purchased from StemExpress or StemCell Technologies. For each experiment, CD34+ cells were first thawed and rested for 48 h in SFEM II with 75 nM StemRegenin 1, 3.5 nM UM729, 1X CC110 (StemCell Technologies), and 1X penicillin-streptomycin (Gibco). To initiate differentiation, cells were cultured in the same medium supplemented with 20% pooled human serum (SeraCare) with or without cytokines at the indicated concentrations for each experiment. Recombinant human IL-24, OSM, IL-33, RETN, OPG, TRAIL, TNFβ, IL-6, IL-10, GM-CSF, M-CSF, and G-CSF were obtained from Peprotech. Cytokines were selected among the top 20 proteins that correlated with changes in EM score in COVACTA (Supplementary Data 3) and those previously shown to induce MS1 monocytes[23]. To assess myelopoiesis, cells were stained with the following panel: CD14-FITC (clone M5E2), CD15-APC (clone W6D3), CD11b-AF700 (clone ICRF44), CD34-BV650 (clone 561), HLA-DR-PE/Cy7 (clone L243) (BioLegend), and IL1R2-PE (clone 34141; Thermo). After staining, cells were resuspended in FACS buffer with 5% CountBright beads (Invitrogen) to allow determination of absolute counts during analysis. Flow cytometry data were acquired on an LSR Fortessa (BD Biosciences) and analyzed using FlowJo v10.10 and GraphPad Prism 10.

COVACTA clinical trial
Details of the COVACTA study have been previously published[40,53]. Briefly, 438 hospitalized COVID-19 patients, confirmed with a positive SARS-CoV-2 PCR test, were randomized 2:1 for anti-interleukin-6 receptor antibody, tocilizumab, or placebo. The NIH COVID-19 ordinal severity scale was used to assess disease severity (3 = hospitalized not requiring supplemental O_2, 4 = supplemental O_2, 5 = non-invasive/high flow O_2, 6 = mechanical ventilation, 7 = mechanical ventilation + additional organ support). Serum protein measurements were obtained using the Olink Explore platform

(Olink), and RNA-seq libraries were generated using the TruSeq Stranded mRNA Library Prep kit (Illumina).

scRNA-seq and data analysis

scRNA-seq combined with cell hashing[54] was performed as previously described[23]. Briefly, cells from multiple culture conditions were labeled with hashtag oligo antibodies (BioLegend) and loaded on the Chromium platform using the 3′ v3 profiling chemistry (10X Genomics). Libraries were sequenced to a depth of ~25,000 reads per cell on a NovaSeq S4 (Illumina). The data were aligned to the GRCh38 reference genome using cellranger v3.1 (10X Genomics). Single-cell data analysis was performed using scanpy with the same preprocessing and filtering parameters described in a prior publication[23]. cNMF was performed using the same parameters detailed above. MS1, NS1, and MHC-II scores were calculated for the top 30 genes in each module (Supplementary Data 1, 2) using the "score_genes" function on scanpy (ctrl_size = 50, n_bins = 25). To analyze mouse scRNA-seq experiments, we first converted the gene expression matrix using mousipy v0.1.5.

Influenza infection in vivo

Wild-type C57BL/6 mice and Ccr2-/- mice were purchased from Jackson Laboratories or Charles River Hollister. Mice were infected intranasally with the indicated dose of influenza H1N1 A/PR/8/1934 in 50 μL Dulbecco's Modified Eagle Medium (DMEM) with 2 μg/mL TCPK Trypsin (Thermo) under anesthesia via intraperitoneal injection of 75–80 mg/kg Ketamine and 7.5–15 mg/kg Xylazine. At day 7 post-infection, mice were anesthetized with isoflurane and 500 μL blood was collected by retro-orbital bleeding. After blood collection, mice were euthanized by cervical dislocation while under anesthesia. BALF samples were collected post-euthanasia by instillation and withdrawal of 1 mL PBS into the lung. BALF cells were obtained by centrifugation for 5 min at $400 \times g$, and supernatants were collected for cytokine, sRAGE, and albumin measurements. Neutrophil depletion was performed by intraperitoneal injection of 10 mg/kg anti-Gr1 (clone RB6-8C5, Leinco Technologies) on day 1 or day 3 post-infection, and every 2 days thereafter. Mice were treated with 2.5 mg/kg anti-GCSF (clone 67604, ThermoFisher) and/or 20 mg/kg anti-IL-6R (Genentech) at day 1 post-infection, and every 2 days thereafter. Studies were performed in compliance with the regulations of the Association of Assessment and Accreditation of Laboratory Animal Care.

Cytokine and lung injury measurements

Cytokine levels were measured using the Milliplex Mouse Panel 32-plex (Millipore Sigma). Enzyme-linked immunosorbent assay (ELISA) kits were used to assay mouse albumin (Abcam) and mouse sRAGE (R&D).

Viral load quantification

MDCK-II cells (ECACC) were cultured in EMEM and seeded ($1.5–2 \times 10^4$ cells/well) in black clear-bottom 96-well plates (Corning) to create a monolayer on the following day of viral infection. Five-fold serial dilutions of mouse BALF were carried out in high glucose DMEM (Glucose 4500 mg/L, 0.2% BSA, 1 M HEPES, 100 U/mL Penicillin, 100 μg/mL Streptomycin, 2 mM Glutamax (ThermoFisher Scientific) with 2 μg/mL TCPK Trypsin (Sigma). Mouse BALF dilutions were then added to the cells, followed by incubation at 37 °C for 16–18 h. Cells were then fixed with 100% ice-cold ethanol, blocked with 2% BSA in PBS, and stained with a mouse anti-Influenza A nucleoprotein (Millipore MAB8258). The 96-well plates were then imaged with the Image Express Confocal HT.ai High Content Imaging System (Molecular Devices). Six images of each well were taken followed by quantitative analysis with the MetaExpress 6.0 Program. The dilution which yielded an average of 5–30 positive AF488 events (pfu) was selected and the viral titer in pfu/ml was calculated.

Statistical analysis

Statistical analyses were performed with either GraphPad Prism 10 software or the SciPy statistics package. P values were calculated using two-tailed Wilcoxon rank sum tests for comparisons across patient groups and Mann-Whitney tests for in vitro and in vivo experiments. Benjamini-Hochberg corrections were applied for multiple hypothesis testing where appropriate.

Reporting summary

Further information on research design is available in the Nature Portfolio Reporting Summary linked to this article.

Data availability

External datasets analyzed and their corresponding accession IDs are listed in Supplementary Tables 1 and 3. scRNA-seq datasets generated in this study are available through the Single Cell Portal (SCP3171 and SCP3172). Source data behind the graphs in the paper are provided in Supplementary Data 4–6.

References

1. Rudd, K. E. et al. Global, regional, and national sepsis incidence and mortality, 1990–2017: analysis for the Global Burden of Disease Study. *Lancet* **395**, 200–211 (2020).
2. Gupta, A. et al. Extrapulmonary manifestations of COVID-19. *Nat. Med.* **26**, 1017–1032 (2020).
3. Andargie, T. E. et al. Cell-free DNA maps COVID-19 tissue injury and risk of death and can cause tissue injury. *JCI Insight* **6**, e147610 (2021).
4. Cheng, A. P. et al. Cell-free DNA tissues of origin by methylation profiling reveals significant cell, tissue, and organ-specific injury related to COVID-19 severity. *Med* **2**, 411–422.e5 (2021).
5. Charoensappakit, A. et al. Cell-free DNA as diagnostic and prognostic biomarkers for adult sepsis: a systematic review and meta-analysis. *Sci. Rep.* **13**, 19624 (2023).
6. Williams, B. A., Jones, C. H., Welch, V. & True, J. M. Outlook of pandemic preparedness in a post-COVID-19 world. *NPJ Vaccines* **8**, 178 (2023).
7. Naghavi, M. et al. Global burden of bacterial antimicrobial resistance 1990–2021: a systematic analysis with forecasts to 2050. *Lancet* **404**, 1199–1226 (2024).
8. Kumar, D. et al. Combining baloxavir marboxil with standard-of-care neuraminidase inhibitor in patients hospitalised with severe influenza (FLAGSTONE): a randomised, parallel-group, double-blind, placebo-controlled, superiority trial. *Lancet Infect. Dis.* **22**, 718–730 (2022).
9. Lim, J. J. et al. A phase 2 randomized, double-blind, placebo-controlled trial of MHAA4549A, a monoclonal antibody, plus oseltamivir in patients hospitalized with severe influenza A virus infection. *Antimicrob. Agents Chemother.* **64**, e00352–20 (2020).
10. Hanula, R. et al. Evaluation of oseltamivir used to prevent hospitalization in outpatients with influenza: a systematic review and meta-analysis. *JAMA Intern. Med.* https://doi.org/10.1001/jamainternmed.2023.0699 (2023).
11. Karim, M., Lo, C.-W. & Einav, S. Preparing for the next viral threat with broad-spectrum antivirals. *J. Clin. Invest.* **133**, e170236 (2023).
12. Tripathi, D., Sodani, M., Gupta, P. K. & Kulkarni, S. Host directed therapies: COVID-19 and beyond. *Curr. Res. Pharmacol. Drug Discov.* **2**, 100058 (2021).
13. Kaufmann, S. H. E., Dorhoi, A., Hotchkiss, R. S. & Bartenschlager, R. Host-directed therapies for bacterial and viral infections. *Nat. Rev. Drug Discov.* **17**, 35–56 (2018).
14. Wallis, R. S., O'Garra, A., Sher, A. & Wack, A. Host-directed immunotherapy of viral and bacterial infections: past, present and future. *Nat. Rev. Immunol.* **23**, 121–133 (2023).
15. Hackney, J. A. et al. A myeloid program associated with COVID-19 severity is decreased by therapeutic blockade of IL-6 signaling. *iScience* **26**, 107813 (2023).

16. Schulte-Schrepping, J. et al. Severe COVID-19 Is Marked by a Dysregulated Myeloid Cell Compartment. *Cell* **182**, 1419–1440.e23 (2020).

17. COvid-19 Multi-omics Blood ATlas (COMBAT) Consortium A blood atlas of COVID-19 defines hallmarks of disease severity and specificity. *Cell* **185**, 916–938.e58 (2022).

18. Dunning, J. et al. Progression of whole-blood transcriptional signatures from interferon-induced to neutrophil-associated patterns in severe influenza. *Nat. Immunol.* **19**, 625–635 (2018).

19. Tang, B. M. et al. Neutrophils-related host factors associated with severe disease and fatality in patients with influenza infection. *Nat. Commun.* **10**, 3422 (2019).

20. Chen, S. T. et al. A shift in lung macrophage composition is associated with COVID-19 severity and recovery. *Sci. Transl. Med.* **14**, eabn5168 (2022).

21. Reyes, M. et al. An immune-cell signature of bacterial sepsis. *Nat. Med.* **26**, 333–340 (2020).

22. Merad, M., Blish, C. A., Sallusto, F. & Iwasaki, A. The immunology and immunopathology of COVID-19. *Science* **375**, 1122–1127 (2022).

23. Reyes, M. et al. Plasma from patients with bacterial sepsis or severe COVID-19 induces suppressive myeloid cell production from hematopoietic progenitors in vitro. *Sci. Transl. Med.* **13**, eabe959 (2021).

24. Leite, G. G. F. et al. Monocyte state 1 (MS1) cells in critically ill patients with sepsis or non-infectious conditions: association with disease course and host response. *Crit. Care* **28**, 88 (2024).

25. Kwok, A. J. et al. Neutrophils and emergency granulopoiesis drive immune suppression and an extreme response endotype during sepsis. *Nat. Immunol.* **24**, 767–779 (2023).

26. Wilk, A. J. et al. Multi-omic profiling reveals widespread dysregulation of innate immunity and hematopoiesis in COVID-19. *J. Exp. Med.* **218**, e20210582 (2021).

27. Sinha, S. et al. Dexamethasone modulates immature neutrophils and interferon programming in severe COVID-19. *Nat. Med.* https://doi.org/10.1038/s41591-021-01576-3 (2021).

28. Qiu, X. et al. Dynamic changes in human single-cell transcriptional signatures during fatal sepsis. *J. Leukoc. Biol.* **110**, 1253–1268 (2021).

29. Ren, X. et al. COVID-19 immune features revealed by a large-scale single-cell transcriptome atlas. *Cell* **184**, 1895–1913.e19 (2021).

30. Stephenson, E. et al. Single-cell multi-omics analysis of the immune response in COVID-19. *Nat. Med.* **27**, 904–916 (2021).

31. van der Wijst, M. G. P. et al. Type I interferon autoantibodies are associated with systemic immune alterations in patients with COVID-19. *Sci. Transl. Med.* https://doi.org/10.1126/scitranslmed.abh2624 (2021).

32. Combes, A. J. et al. Global absence and targeting of protective immune states in severe COVID-19. *Nature* **591**, 124–130 (2021).

33. Liu, C. et al. Time-resolved systems immunology reveals a late juncture linked to fatal COVID-19. *Cell* **184**, 1836–1857.e22 (2021).

34. Lee, J. S. et al. Immunophenotyping of COVID-19 and influenza highlights the role of type I interferons in development of severe COVID-19. *Sci. Immunol.* **5**, eabd1554 (2020).

35. Arunachalam, P. S. et al. Systems biological assessment of immunity to mild versus severe COVID-19 infection in humans. *Science* **369**, 1210–1220 (2020).

36. Wilk, A. J. et al. A single-cell atlas of the peripheral immune response in patients with severe COVID-19. *Nat. Med.* **26**, 1070–1076 (2020).

37. Jiang, Y. et al. Single cell RNA sequencing identifies an early monocyte gene signature in acute respiratory distress syndrome. *JCI Insight* **5**, e135678 (2020).

38. Bernardes, J. P. et al. Longitudinal multi-omics analyses identify responses of megakaryocytes, erythroid cells, and plasmablasts as hallmarks of severe COVID-19. *Immunity* **53**, 1296–1314.e9 (2020).

39. Hoogendijk, A. J. et al. Dynamic transcriptome-proteome correlation networks reveal human myeloid differentiation and neutrophil-specific programming. *Cell Rep.* **29**, 2505–2519.e4 (2019).

40. Shivram, H. et al. Transcriptomic and proteomic assessment of tocilizumab response in a randomized controlled trial of patients hospitalized with COVID-19. *iScience* **26**, 107597 (2023).

41. Metcalf, D. The granulocyte-macrophage colony-stimulating factors. *Science* **229**, 16–22 (1985).

42. Mehta, H. M. & Corey, S. J. G-CSF, the guardian of granulopoiesis. *Semin. Immunol.* **54**, 101515 (2021).

43. Leisman, D. E. et al. Alveolar, endothelial, and organ injury marker dynamics in severe COVID-19. *Am. J. Respir. Crit. Care Med.* https://doi.org/10.1164/rccm.202106-1514OC (2021).

44. Jabaudon, M. et al. Soluble receptor for advanced glycation end-products predicts impaired alveolar fluid clearance in acute respiratory distress syndrome. *Am. J. Respir. Crit. Care Med.* **192**, 191–199 (2015).

45. Zheng, H. et al. Multi-cohort analysis of host immune response identifies conserved protective and detrimental modules associated with severity across viruses. *Immunity* **54**, 753–768.e5 (2021).

46. Eddins, D. J. et al. Transcriptional reprogramming of infiltrating neutrophils drives lung pathology in severe COVID-19 despite low viral load. *Blood Adv.* **7**, 778–799 (2023).

47. Zhang, J. et al. Interleukin-6 and granulocyte colony-stimulating factor as predictors of the prognosis of influenza-associated pneumonia. *BMC Infect. Dis.* **22**, 343 (2022).

48. Vanderbeke, L. et al. Monocyte-driven atypical cytokine storm and aberrant neutrophil activation as key mediators of COVID-19 disease severity. *Nat. Commun.* **12**, 4117 (2021).

49. Veras, F. P. et al. SARS-CoV-2-triggered neutrophil extracellular traps mediate COVID-19 pathology. *J. Exp. Med.* **217**, e20201129 (2020).

50. Veras, F. P. et al. Targeting neutrophils extracellular traps (NETs) reduces multiple organ injury in a COVID-19 mouse model. *Respir. Res.* **24**, 66 (2023).

51. Cardot-Ruffino, V. et al. G-CSF rescue of FOLFIRINOX-induced neutropenia leads to systemic immune suppression in mice and humans. *J. Immunother. Cancer* **11**, e006589 (2023).

52. Lee, Y. S., Saxena, V., Bromberg, J. S. & Scalea, J. R. G-CSF promotes alloregulatory function of MDSCs through a c-Kit dependent mechanism. *Cell. Immunol.* **364**, 104346 (2021).

53. Rosas, I. O. et al. Tocilizumab in hospitalized patients with severe Covid-19 pneumonia. *N. Engl. J. Med.* **384**, 1503–1516 (2021).

54. Stoeckius, M. et al. Cell Hashing with barcoded antibodies enables multiplexing and doublet detection for single cell genomics. *Genome Biol.* **19**, 224 (2018).

55. Hoang, L. T. et al. Patient-based transcriptome-wide analysis identify interferon and ubiquination pathways as potential predictors of influenza A disease severity. *PLoS ONE* **9**, e111640 (2014).

56. Ramilo, O. et al. Gene expression patterns in blood leukocytes discriminate patients with acute infections. *Blood* **109**, 2066–2077 (2007).

57. de Steenhuijsen Piters, W. A. A. et al. Nasopharyngeal microbiota, host transcriptome, and disease severity in children with respiratory syncytial virus infection. *Am. J. Respir. Crit. Care Med.* **194**, 1104–1115 (2016).

Acknowledgements

Author contributions

Experiments: K.K., D.Y., G.L.S., H.L.-H., J.K., C.C, M.D.S., T.D., and M.R.; Computational Analysis: H.S. and M.R.; Data Curation: H.S., R.N.B., C.M.R., and M.R.; Supervision: S.D., R.N.B., C.M.R., S.B.K., M.X., and M.R.; Conceptualization: C.M.R., S.B.K., M.X., and M.R.; Manuscript Writing: K.K., G.L.S., and M.R.; Manuscript Review and Editing: all authors.

Competing interests

All authors are employees of Genentech, Inc. at the time of this study and own equity in Roche.

Additional information

Supplementary information The online version contains supplementary material available at https://doi.org/10.1038/s42003-025-08407-y.

Correspondence and requests for materials should be addressed to Miguel Reyes.

Peer review information *Communications Biology* thanks the anonymous reviewers for their contribution to the peer review of this work.

Reprints and permissions information is available at http://www.nature.com/reprints

Publisher's note Springer Nature remains neutral with regard to jurisdictional claims in published maps and institutional affiliations.